

# Design of Tone-Dependent Color-Error Diffusion Halftoning Systems

Vishal Monga, *Member, IEEE*, Niranjan Damera-Venkata, *Member, IEEE*, and Brian L. Evans, *Senior Member, IEEE*

**Abstract**—Grayscale error diffusion introduces nonlinear distortion (directional artifacts and false textures), linear distortion (sharpening), and additive noise. Tone-dependent error diffusion (TDED) reduces these artifacts by controlling the diffusion of quantization errors based on the input graylevel. We present an extension of TDED to color. In color-error diffusion, which color to render becomes a major concern in addition to finding optimal dot patterns. We propose a visually meaningful scheme to train input-level (or tone-) dependent color-error filters. Our design approach employs a Neugebauer printer model and a color human visual system model that takes into account spatial considerations in color reproduction. The resulting halftones overcome several traditional error-diffusion artifacts and achieve significantly greater accuracy in color rendition.

**Index Terms**—Color halftoning, color image display and printing, error diffusion.

## I. INTRODUCTION

**D**IGITAL halftoning is the process of representing continuous-tone (a.k.a. grayscale and color) images with a finite number of levels for the purpose of display or printing on devices with finite reproduction palettes. Examples include conversion of a 24-bit color image to a three-bit color image and conversion of an 8-bit grayscale image to a binary image.

Halftoning methods in current use may be categorized as classical screening, dithering with blue noise, direct binary search (DBS), and error diffusion. Classical screening, which is the oldest halftoning method in printing, applies a periodic array of thresholds to each color of the multibit image. Pixels can be converted to 255 (black) if they are above the threshold or 0 (white) otherwise. The human visual system may be roughly approximated as a linear spatially invariant (LSI) system that is lowpass to the luminance component of a color image. Dithering with blue noise (i.e., high-frequency noise) [1] attempts to place the quantization noise from the halftoning process into the higher frequencies. Noise shaping is a characteristic of error diffusion as described later, but large periodic masks of thresholds (e.g.,

$128 \times 128$  pixels) can be designed to produce halftones with blue noise [2], [3]. Although a plethora of screen design techniques have been proposed [4], they do not produce halftone image quality comparable to DBS.

Direct binary search [5] produces blue noise halftones by iteratively searching for the best binary pattern to match a given grayscale image by minimizing a distortion criterion. The distortion criterion incorporates a linear spatially invariant model of the human visual system as a weighting function [6]. The direct binary search method produces halftones with the highest visual quality to date. Due to its implementation complexity, it is impractical for use as a halftoning method in desktop printers. However, direct binary search can be employed to design screens [7] and error-diffusion parameters.

Error diffusion produces halftones of much higher quality than classical screening, with the tradeoff of requiring more computation and memory [8], [9]. Screening amounts to pixel-parallel thresholding, whereas error diffusion requires a neighborhood operation and thresholding. The neighborhood operation distributes the quantization error due to thresholding to the unhalftoned neighbors of the current pixel. The term “error diffusion” refers to the process of diffusing the quantization error along the path of the image scan; e.g., in the case of a raster scan, the quantization error diffuses across and down the image. This diffusion of errors occurs in a feedback arrangement [8], which causes the quantization error to be highpass filtered.

Classical error diffusion as proposed in [8], however, introduces nonlinear distortion (worms and false textures), linear distortion (sharpening), and additive noise [10]. Many variations and enhancements have been developed to improve halftone quality for grayscale error diffusion, which includes threshold modulation [11]–[16], variable error filter weights [9], [17]–[19], and different scan paths [9], [20].

Recently, tone-dependent methods have been developed for grayscale error diffusion [21]–[24]. These methods use error filters with different coefficients for different graylevels in the input image. The quantizer threshold is also modulated based on the input graylevel [24]. The fundamental premise behind the approaches in [21]–[24] was to identify that qualitatively, error diffusion reproduces an input tone (or graylevel) in a local region by driving the average error to zero. An optimization for each input tone would, hence, enhance the feedback mechanism to more accurately determine the correct (or optimum) amount of error to diffuse.<sup>1</sup>

In this paper, we formulate the design of input-level or tone-dependent color-error diffusion halftoning systems. In particular, we focus on design issues that differentiate color-error

Manuscript received November 20, 2004; revised June 7, 2006. The associate editor coordinating the review of this manuscript and approving it for publication was Dr. Reiner Eschbach.

V. Monga is with the Xerox Wilson Research Center, Webster, NY 14580 USA (e-mail: vishal.monga@xerox.com).

N. Damera-Venkata is with the Hewlett Packard Laboratories, Palo Alto, CA 94394 USA (e-mail: niranjan.damera-venkata@hp.com).

B. L. Evans is with the Embedded Signal Processing Laboratory, Department of Electrical and Computer Engineering, The University of Texas at Austin, Austin, TX 78712 USA (e-mail: bevans@ece.utexas.edu).

Color versions of Figs. 2, 4, and 7–14 are available online at <http://ieeexplore.ieee.org>.

Digital Object Identifier 10.1109/TIP.2006.884923

<sup>1</sup>Work presented in part at the IEEE ICASSP, May 2004.

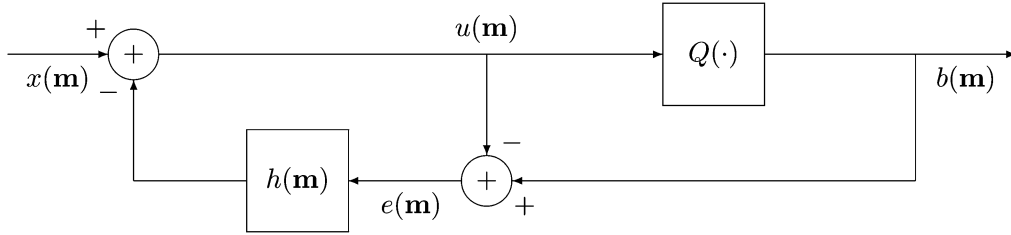


Fig. 1. System block diagram for grayscale error-diffusion halftoning where  $\mathbf{m}$  represents a 2-D spatial index  $(m_1, m_2)$  and  $h(\mathbf{m})$  is the impulse response of a fixed 2-D nonseparable FIR error filter.

diffusion from its grayscale counterpart. An independent design for each color plane would ignore the correlation among color planes and can often result in inaccurate color reproduction [25]. We motivate this problem by asking the following question: “Suppose we want to print a patch of solid color, what colors should we use?” Traditional work on halftoning addresses the issue of what pattern should the dots be placed in. The issue of participating halftone color was raised in [26], but it served primarily as an example of how bad things can become. A few previous efforts in color-error diffusion have addressed this problem to some extent. These include color plane separable design and implementation of error diffusion [18], vector quantization based on perceptual criterion [27]–[29] and non-separable processing of color planes via matrix valued filters [30], [31].

This paper proposes a more complete answer to the issue. In particular, we observe that the accuracy of color rendition in halftoning by error diffusion can be significantly enhanced by optimizing error filters based on the input colorant (CMY) or tone values. However, the notion of “tone” in the case of color is far more involved. To optimize over the entire color gamut, one needs to design error filters for all possible input CMY combinations. This number easily grows to be prohibitively large; e.g., for 24-bit color images with 8-bits per color plane there are  $(256)^3$  different combinations. It is, therefore, needed to constrain the design to regions in the CMY color cube that are critical to color reproduction. Further, these regions must ideally be specified in device-independent and visually meaningful coordinates (e.g., in the CIELab space [32]) so that the color quantization error may be diffused to frequencies and colors to which the eye is least sensitive.

We design error filters for CMY combinations that correspond to the true neutrals in the device-independent gamut, i.e., the locus  $(L^*, 0, 0)$  in the CIELab space. Our design procedure then trains error filter weights in order to minimize the perceived error between a constant-valued continuous-tone color image and its corresponding halftone pattern. A color human visual system (HVS) model takes into account the correlation among color planes. We employ an HVS model based on a transformation to the Linearized CIELab color space [33] that exploits the spatial frequency sensitivity variation of the luminance and chrominance channels. The efficacy of Linearized CIELab in computing color reproduction errors in halftoning is shown in [31]. The resulting halftones overcome many artifacts associated with traditional error diffusion *viz.* worms and false textures. The most significant gain, however, lies in a much smaller

perceived error between the colors in a continuous tone image and its corresponding halftone pattern versus separable design schemes. The color HVS model also helps minimize the visibility of the halftone pattern.

The rest of the paper is organized as follows. Section II-A outlines the basic structure of error diffusion. In Section II-B, we briefly describe the tone-dependent error diffusion (TDED) algorithm by Li and Allebach [24] for halftoning grayscale images. Section III reviews previous work in color-error diffusion and further motivates our approach. Our proposed approach for designing input-level or tone-dependent color-error filters is then described in Section IV. Section V compares halftone images generated by our algorithm with other schemes in the literature and analyzes the findings. Some possible enhancements are considered in Section VI. Section VII summarizes the paper.

## II. GRAYSCALE ERROR-DIFFUSION HALFTONING

### A. Classical Error Diffusion

In grayscale halftoning by error diffusion, each grayscale pixel is thresholded to white or black, and the quantization error is fed back, filtered and added to the neighboring grayscale pixels [8]. The system block diagram shown in Fig. 1 is also known as a noise-shaping feedback coder. In Fig. 1,  $x(\mathbf{m})$  denotes the graylevel of the input image at pixel location  $\mathbf{m}$ , such that  $x(\mathbf{m}) \in [0, 255]$ . The output halftone pixel is  $b(\mathbf{m})$ , where  $b(\mathbf{m}) \in \{0, 255\}$ . Here, 0 is interpreted as the absence of a printer dot and 255 is interpreted as the presence of a printer dot.  $Q(\cdot)$  denotes the standard thresholding quantizer function.

The error filter  $h(\mathbf{m})$  filters the previous quantization errors  $e(\mathbf{m})$

$$h(\mathbf{m}) * e(\mathbf{m}) = \sum_{\mathbf{k} \in \mathcal{S}} h(\mathbf{k}) e(\mathbf{m} - \mathbf{k}). \quad (1)$$

Here,  $*$  means linear convolution, and the set  $\mathcal{S}$  defines the extent of the error filter coefficient mask. The error filter output is fed back and added to the input. Note that  $(0, 0) \notin \mathcal{S}$ . The mask is causal with respect to the image scan. To ensure that all of the quantization error is diffused,  $h(\mathbf{m})$  must satisfy the constraint

$$\sum_{\mathbf{k} \in \mathcal{S}} h(\mathbf{k}) = 1. \quad (2)$$

This constraint ensures that the error filter eliminates quantization noise at DC where the human visual system is most sensi-

tive [34]. The quantizer input  $u(\mathbf{m})$  and output  $b(\mathbf{m})$  are given by

$$u(\mathbf{m}) = x(\mathbf{m}) - h(\mathbf{m}) * e(\mathbf{m}) \quad (3)$$

$$b(\mathbf{m}) = Q(u(\mathbf{m})). \quad (4)$$

Error diffusion produces high-quality halftones because the quantization noise is shaped into the high frequencies where the human eye is less sensitive. Since the halftone dots are of single pixel size, the illusion of continuous-tone is created by varying the dot frequency with graylevel.

### B. Grayscale Tone-Dependent Error Diffusion

TDED methods use error filters  $h(\mathbf{m})$  of different sizes and coefficients for different graylevels [21], [24]. Optimal error weighting for selected graylevels based on “blue-noise” spectra was introduced in [35].

Li *et al.* design error filter weights and thresholds so that the resulting halftones approximate dot patterns generated by DBS. DBS [5] produces high-quality halftones by searching for the best binary pattern to match a given grayscale image by minimizing a visual distortion criterion. For the TDED algorithm in [24], the error filter and threshold matrix, denoted by  $h(\mathbf{m})$  and  $t(\mathbf{m}; d)$  respectively, are functions of input pixel value  $d \in [0, 255]$ . The binary output  $b(\mathbf{m})$  is determined by

$$b(\mathbf{m}) = \begin{cases} 255, & \text{if } u(\mathbf{m}) \geq t(\mathbf{m}; x(\mathbf{m})) \\ 0, & \text{otherwise.} \end{cases} \quad (5)$$

The quantization error  $e(\mathbf{m})$  and the quantizer input  $u(\mathbf{m})$  are then computed as in conventional grayscale error diffusion. The threshold matrix used by Li and Allebach [24] is based on a binary DBS pattern for a constant input of mid-gray

$$t(\mathbf{m}; d) = \begin{cases} t_u(d), & \text{if } p[\mathbf{m}, 128] = 0 \\ t_l(d), & \text{otherwise.} \end{cases} \quad (6)$$

where  $t_u(d)$  and  $t_l(d)$  are tone-dependent parameters satisfying  $t_u(d) \geq t_l(d)$ . The function  $p[\mathbf{m}, 128]$  is a halftone pattern generated by DBS that represents a constant patch of mid-gray. By substituting (6) into (5), the thresholding process can be represented by

$$b(\mathbf{m}) = \begin{cases} 255, & \text{if } u(\mathbf{m}) \geq t_u(x(\mathbf{m})) \\ 0, & \text{if } u(\mathbf{m}) < t_l(x(\mathbf{m})) \\ p[\mathbf{m}, 128], & \text{otherwise.} \end{cases} \quad (7)$$

For the error filter design, the authors chose the magnitude of the DFT of the DBS pattern as an objective spectrum for the halftone pattern for input graylevel values in the midtones (21–234). For the highlight and shadow regions (graylevel values in 0–20 and 235–255) the objective spectrum is the DFT of the graylevel patch. Let  $B^{\text{DBS}}(k, l)$  and  $B^{\text{TDED}}(k, l)$  denote the DFT of the DBS and the TDED patterns, respectively. The

goal is then to search for the tone-dependent parameter vector  $v = (t_u(d), t_l(d), h(\mathbf{m}; d))$  that minimizes

$$J = \sum_k \sum_l (|B^{\text{TDED}}(k, l)| - |B^{\text{DBS}}(k, l)|)^2 \quad (8)$$

subject to the constraints

$$t_u(d) + t_l(d) = 255 \quad (9)$$

$$t_u(d) \geq t_l(d) \quad (10)$$

$$\sum_{\mathbf{k} \in \mathcal{S}} h(\mathbf{k}; d) = 1 \quad (11)$$

$$h(\mathbf{k}; d) \geq 0 \quad \forall \mathbf{k} \in \mathcal{S}. \quad (12)$$

Note that  $B^{\text{DBS}}(k, l)$  would be replaced by  $X(k, l)$  (the DFT of the input graylevel patch) for the highlight and shadow regions. The difference  $|B^{\text{TDED}}(k, l)| - |X(k, l)|$  is then weighted (convolved) by a human visual system frequency response [5] to compute the perceived error. The algorithm to search for the optimum tone-dependent parameter vector  $v_{\text{opt}}$  is described in [24].

### III. PREVIOUS WORK IN COLOR-ERROR DIFFUSION

Kolpatzik and Bouman [18] use separable error filters in a luminance-chrominance space to account for correlation among the color planes. Separate optimum scalar error filters are designed for the luminance and chrominance channels independently based on a separable model of the human visual system. However, no constraints are imposed on the error filter to ensure that all of the red-green-blue (RGB) (or CMY) quantization error is diffused.

Haneishi *et al.* [27] suggested the use of the CIEXYZ and CIELab spaces to perform quantization and error diffusion. In this case the rendering gamut is no longer a cube. The mean-squared error (MSE) criterion in the XYZ or Lab space is used to make a decision on the best color to output. The quantization error is a vector in the XYZ space and is diffused using an error filter (lab space is not suitable for diffusing errors due to its nonlinear variation with intensity). This method performs better than separable quantization but suffers from boundary artifacts [27], [28] such as the “smear artifact” and the “slow response artifact” at color boundaries due to accumulated errors from neighboring pixels pushing quantizer input colors outside the gamut. This effect may be reduced by clipping large color errors [27], [29] or by using a hybrid scalar-vector quantization method called semi-vector quantization [28]. Error diffusion and perceptual quantization in device independent spaces also significantly increases the computational complexity since nonlinear color transformations and gamut mapping would now become a part of the error-diffusion loop.

Another significant improvement to separable color halftoning involves limiting the number of ink colors used to render a specific pixel. Shaked *et al.* [36], [37] suggest a method for using error diffusion for generating color halftone patterns that carefully examines each pixel’s original color values simultaneously, distinct from past error, in order to determine potential output colors. By limiting the colors used,

the authors argue that a smaller range of brightnesses in the colors are used to create each color area, which minimizes the visibility of the halftone pattern. This criteria, which is known as the minimum brightness variation criterion (MBVC), is based on the observation that the human eye is more sensitive to changes in “brightness” or luminance than to changes in chrominance.

Finally, Damera-Venkata and Evans [30] proposed using *matrix valued* filters to take into account the correlation among color planes. They extended the (linear) scalar gain model used in analyzing grayscale error diffusion proposed by Kite *et al.* [38] to a (linear) matrix gain model for color images. The matrix valued error filters were designed to minimize the visually weighted energy in response to the quantization error which was modelled as additive uncorrelated noise [30]. For an RGB image, each error filter coefficient would be a  $3 \times 3$  matrix.

In the proposed work, we present a nonseparable design that obtains visually optimum color-error filters for each of the  $C$ ,  $M$  and  $Y$  channels that are *dependent* on the input CMY triplet (or tone). We constrain the error filters so that the entire cyan, magenta and yellow quantization error is diffused. The design approach is model based. A Neugebauer printer model [39] is employed for predicting the colorimetric response of the printer and a color HVS model is used to compute the perceived error in color reproduction. We show that by designing color-error filters dependent on a small number of cleverly chosen “canonical” CMY combinations we can achieve significantly improved color accuracy all over the device gamut.

#### IV. TONE-DEPENDENT COLOR-ERROR DIFFUSION

We aim to minimize color reproduction errors (spatial considerations included) in a visually meaningful color space i.e., Linearized CIELab [33]. This requires the availability of a reasonably accurate transformation from the device-dependent coordinates, i.e., printer CMY to our desired color space. We employ the widely used Neugebauer printer model [39] for this purpose which is briefly reviewed. Then, we detail our design approach to train and optimize error filters along each of the colorant planes.

##### A. Printer Characterization via the Neugebauer Model

The Neugebauer printer model has been successfully used by several researchers to model a halftone color printing process. For such a printer, the rendering of a multitude of colors is achieved through combinations of varying dot area coverages of the primary colorants. The Neugebauer equations [39] predict the average spectral reflectance from an arbitrary printed patch as a weighted average of the spectral reflectances of  $2^N$  known basis colors. In this work, we will focus on the case of CMY printers, i.e.,  $N = 3$ . Our design methodology is easily generalized to  $N > 3$  colorants.

For CMY printers, there are eight basis colors, which are the white paper (W), and the 1, 2, and 3 solid color overlays (i.e., 0% and 100% combinations) of  $C$ ,  $M$ ,  $Y$ . These basis colors are commonly referred to as the Neugebauer primaries. In the original Neugebauer equations, the color being predicted is specified by three broadband reflectances representing the short, medium and long wavelength portions of the electromagnetic spectrum. In this work, spectrally narrowband reflectances  $R(\lambda)$  are used instead of their broadband counterparts, since the former generally yields greater accuracy [40]. For a given digital input  $[C, M, Y]$  with corresponding area coverages  $c$ ,  $m$ ,  $y$  ( $0 < c, m, y < 1$ ), the spectral Neugebauer equations predict the average spectral reflectance of the printed sample to be

$$\hat{R}(\lambda)_{cmY} = \sum_{i=1}^8 w_i(c, m, y) P_i(\lambda) \quad (13)$$

where  $P_i(\lambda)$  represent the measured spectral reflectances of the Neugebauer primaries and  $w_i(c, m, y)$  is the weight of the  $i^{\text{th}}$  primary. These weights are determined by the dot placement or dot overlap model. We select weights based on Demichel dot model [41] which assumes a random dot placement typical of rotated halftone screens and error diffusion.

Yule and Nielsen [42] proposed a simple correction to the above model in (13) that accounts for light scattering in paper

$$\hat{R}(\lambda)_{cmY} = \left[ \sum_{i=1}^8 w_i(c, m, y) P_i(\lambda)^{(1/n)} \right]^n \quad (14)$$

where  $n$  is referred to as the Yule-Nielsen (Y-N) factor. Although, the Y-N correction was originally proposed to account for light scattering it has been found [43] to even account for other physical factors such as halftone screen frequency and measurement noise. The approach taken in our work was to optimize the Y-N factor as a free parameter so that predicted printer response agrees as much as possible with the true (measured) printer response.

##### B. Perceptual Error Metric

We train error filters to minimize a visually weighted squared error between the magnitude spectra of a “constant” input color image and its halftone pattern. Let  $x_{(C,M,Y)}(\mathbf{m})$  and  $b_{(C,M,Y)}(\mathbf{m})$  denote the constant valued continuous tone and halftone images, respectively.  $x_{(Y_y, C_x, C_z)}(\mathbf{m})$  and  $b_{(Y_y, C_x, C_z)}(\mathbf{m})$  are obtained by transforming  $x_{(C,M,Y)}(\mathbf{m})$  and  $b_{(C,M,Y)}(\mathbf{m})$  to the  $Y_y C_x C_z$  (or Linearized CIELab) color space. This transformation is made in the equation at the bottom of the page. The first transformation, from printer CMY to spectral reflectances, is based on the printer model look up table (LUT) implementation of (14). The transformation from

spectral reflectances to CIEXYZ can be found in standard color literature [32]. The linearized CIELab color space may be obtained from the CIEXYZ space in the following manner [33]:

$$Y_y = 116 \frac{Y}{Y_n} - 16 \quad (15)$$

$$C_x = 500 \left[ \frac{X}{X_n} - \frac{Y}{Y_n} \right] \quad (16)$$

$$C_z = 200 \left[ \frac{Y}{Y_n} - \frac{Z}{Z_n} \right]. \quad (17)$$

The  $Y_y$  component is proportional to the luminance and the  $C_x$  and  $C_z$  components are similar to the red-green and blue-yellow opponent color chrominance components on which Mullen's data [44] is based. The original transformation to the CIELab from CIEXYZ is a nonlinear one

$$L^* = 116f\left(\frac{Y}{Y_n}\right) - 16 \quad (18)$$

$$a^* = 500 \left[ f\left(\frac{X}{X_n}\right) - f\left(\frac{Y}{Y_n}\right) \right] \quad (19)$$

$$b^* = 200 \left[ f\left(\frac{Y}{Y_n}\right) - f\left(\frac{Z}{Z_n}\right) \right] \quad (20)$$

where

$$f(x) = \begin{cases} 7.787x + \frac{16}{116} & \text{if } 0 \leq x \leq 0.008856 \\ x^{1/3} & \text{if } 0.008856 < x \leq 1. \end{cases}$$

The values for  $X_n$ ,  $Y_n$ , and  $Z_n$  are as per the D65 white point [45].

The nonlinearity in the transformation from CIELab distorts the spatially averaged tone of the images, which yields halftones that have incorrect average values [33]. The linearized color space overcomes this, and has the added benefit that it decouples the effect of incremental changes in  $(Y_y, C_x, C_z)$  at the white point on  $(L^*, a^*, b^*)$  values

$$\nabla_{(Y_y, C_x, C_z)}(L^*, a^*, b^*)|_{D65} = \frac{1}{3}\mathbf{I}. \quad (21)$$

The difference in the Fourier spectra of the "constant" input image and its halftone pattern is denoted by  $\xi(k, l)$  and computed as  $\xi(k, l) = \mathbf{X}_{(Y_y, C_x, C_z)}(k, l) - \mathbf{B}_{(Y_y, C_x, C_z)}(k, l)$  where

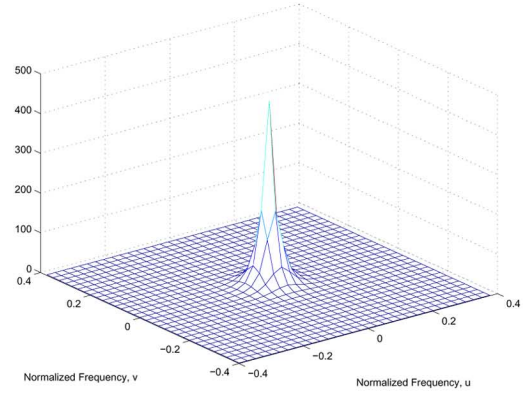
$$\mathbf{X}_{(Y_y, C_x, C_z)}(k, l) = FFT(x_{(Y_y, C_x, C_z)}(\mathbf{m})) \quad (22)$$

$$\mathbf{B}_{(Y_y, C_x, C_z)}(k, l) = FFT(b_{(Y_y, C_x, C_z)}(\mathbf{m})) \quad (23)$$

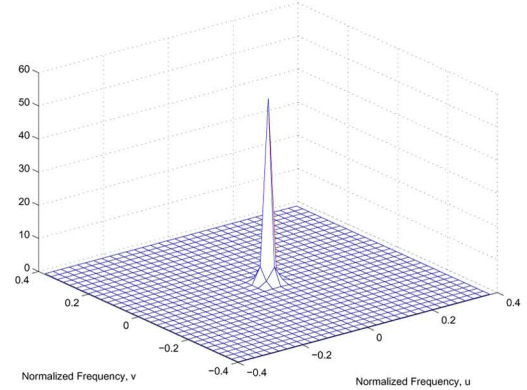
where FFT is the 2-D fast Fourier transform.

We then apply a visual weighting to the luminance and chrominance components of the  $(Y_y, C_x, C_z)$  color-error image. Nasanen and Sullivan [46] chose an exponential function to model the luminance frequency response

$$W_{(Y_y)}(\tilde{\rho}) = K(L)e^{-\alpha(L)\tilde{\rho}} \quad (24)$$



(a)



(b)

Fig. 2. Spatial frequency responses (a) luminance  $W_{(Y_y)}(\mathbf{u})$  and (b) chrominance  $W_{(C_x, C_z)}(\mathbf{u})$ .

where  $L$  is the average luminance of display,  $\tilde{\rho}$  is the radial spatial frequency,  $K(L) = aL^b$ , and

$$\alpha(L) = \frac{1}{c \ln(L) + d}. \quad (25)$$

The frequency variable  $\tilde{\rho}$  is defined [33] as a weighted magnitude of the frequency vector  $\mathbf{u} = (u, v)^T$ , where the weighting depends on the angular spatial frequency  $\phi$  [46]. Thus

$$\tilde{\rho} = \frac{\rho}{s(\phi)} \quad (26)$$

where  $\rho = \sqrt{u^2 + v^2}$  and

$$s(\phi) = \frac{1 - \omega}{2} \cos(4\phi) + \frac{1 + \omega}{2}. \quad (27)$$

The symmetry parameter  $\omega$  is 0.7, and  $\phi = \arctan(v/u)$  [46]. The weighting function  $s(\phi)$  effectively reduces the contrast sensitivity to spatial frequency components at odd multiples of  $45^\circ$ . The contrast sensitivity of the human viewer to spatial variations in chrominance falls off faster as a function of increasing spatial frequency than does the response to spatial variations in

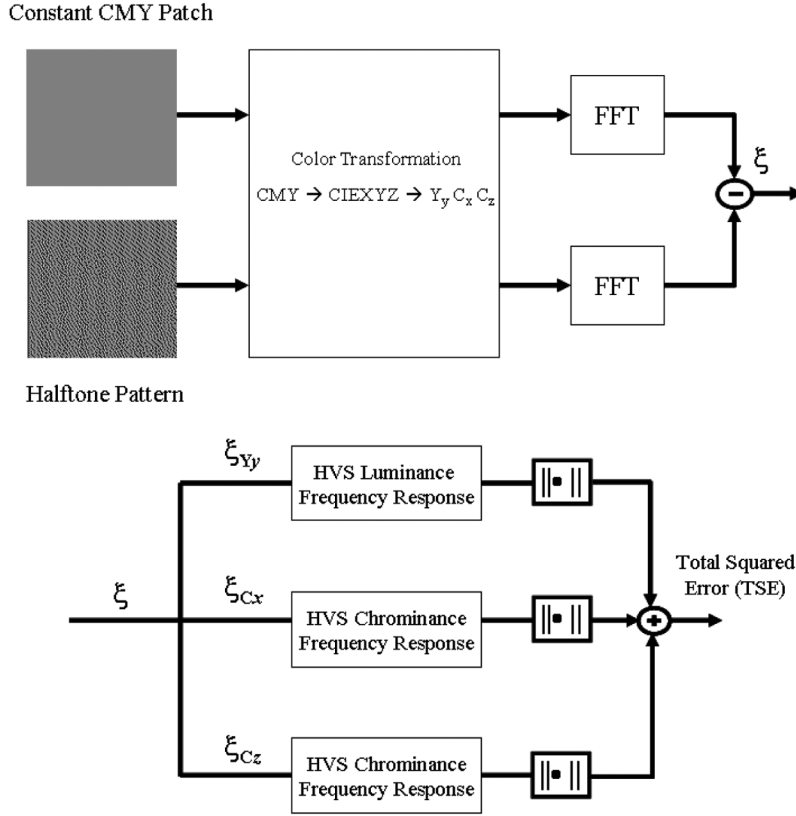


Fig. 3. Block diagram for calculating perceptual error metric.

luminance [47]. We use a chrominance model that reflects this [18]

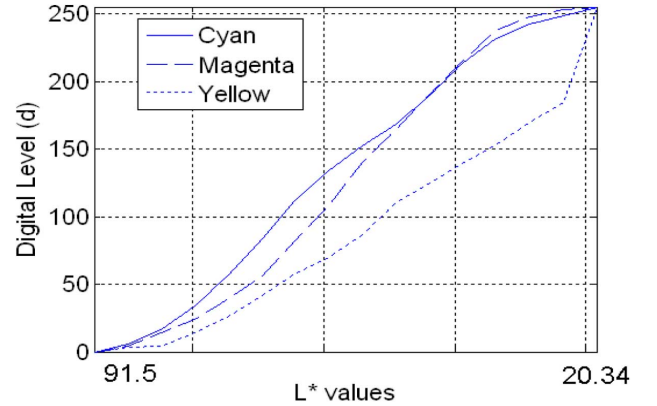
$$W_{(C_x, C_z)}(\rho) = Ae^{-\alpha\rho}. \quad (28)$$

Here,  $\alpha$  is determined to be 0.419 and  $A = 100$  [18]. Both the luminance and chrominance response are lowpass in nature but only the luminance response is reduced at odd multiples of  $45^\circ$  (Fig. 2). This will place more luminance error across the diagonals in the frequency domain where the eye is less sensitive. Using this chrominance response instead of identical responses for both luminance and chrominance associates a greater penalty with mid and low frequency luminance errors as opposed to corresponding chrominance errors. This allows more error to be diffused to the chrominance channels, which will not be perceived by the human viewer.

The aforementioned color HVS filtering is carried out in the spatial frequency domain. This corresponds to a multiplication of the filter and error image spectra  $\mathbf{P}(k, l) = \mathbf{H}_{HVS}(k, l)\xi(k, l)$ . Here,  $\mathbf{H}_{HVS}(k, l)$  denotes the FFT of the HVS response spatial filter. Note,  $\mathbf{P}(k, l)$ ,  $\mathbf{H}_{HVS}(k, l)$  and  $\xi(k, l)$  are vector valued

$$\xi(k, l) = (\xi_{Y_y}(k, l), \xi_{C_x}(k, l), \xi_{C_z}(k, l)) \quad (29)$$

$$\mathbf{H}_{HVS}(k, l) = (H_{Y_y}(k, l), H_{C_x}(k, l), H_{C_z}(k, l)) \quad (30)$$


 Fig. 4.  $C$ ,  $M$ , and  $Y$  values along the neutrals obtained by printer model inversion.

$$\mathbf{P}(k, l) = (P_{Y_y}(k, l), P_{C_x}(k, l), P_{C_z}(k, l)). \quad (31)$$

We define the perceived error metric as the total-squared error (TSE) given by

$$\text{TSE} = \sum_k \sum_l |P_{Y_y}(k, l)|^2 + |P_{C_x}(k, l)|^2 + |P_{C_z}(k, l)|^2. \quad (32)$$

The calculation of the perceptual error metric is illustrated in Fig. 3.

- 1: **Definitions:** Let  $p$  be the vector of “filter weights”. In particular
 
$$p = (h_c(\mathbf{k}; d), h_m(\mathbf{k}; d), h_y(\mathbf{k}; d)) \quad d \in [0, 255], \mathbf{k} = (k_1, k_2), \mathbf{k} \in \mathcal{S}$$
 Let  $p^{(i)}$  denote the value of  $p$  at the  $i^{\text{th}}$  iteration
 
$$\text{Define the neighborhood of } p^{(i)} = (h_c^{(i)}(\mathbf{k}; d), h_m^{(i)}(\mathbf{k}; d), h_y^{(i)}(\mathbf{k}; d)) \text{ as}$$

$$N_\delta(p^{(i)}) = \{(h_c(\mathbf{k}; d), h_m(\mathbf{k}; d), h_y(\mathbf{k}; d)) : |h_l(\mathbf{k}; d) - h_l^{(i)}(\mathbf{k}; d)| \leq \delta, l = c, m, y\}$$
- 2: Set  $p^{(0)}$  (i.e., initial guess) to be the optimized value from the last designed CMY triplet
 

(Note: For the first CMY triplet to design, set  $p^{(0)}$  to Floyd-Steinberg weights)
- 3:  $\delta = \frac{1}{16}$ ,  $i = 0$  and  $\epsilon$  is a user defined parameter
 

while  $(|p^{(i)} - p^{(i-1)}| > \epsilon)$  {

find  $p^{(i+1)} \in N_\delta(p^{(i)})$  that minimizes the total squared error (TSE) in (32)

$i \leftarrow i + 1$  }

while  $(\delta > \frac{1}{512})$  {

$\delta \leftarrow \frac{\delta}{2}$

find  $p^{(i+1)} \in N_\delta(p^{(i)})$  that minimizes the TSE in (32)

$i \leftarrow i + 1$  }
- 4: The optimum  $p$  is  $p_{opt} = p^{(i)}$

Fig. 5. Algorithm to search for optimum input-dependent color-error filters.

### C. Formulation of the Design Problem

The design problem is then to obtain error filters for each color plane that minimize the TSE defined in (32), subject to the constraints that all quantization error to be diffused

$$\sum_{\mathbf{k} \in \mathcal{S}} h_l(\mathbf{k}; d) = 1, h_l(\mathbf{k}; d) \geq 0 \quad \forall \mathbf{k} \in \mathcal{S} \quad (33)$$

where the subscript  $l$  takes on values  $C$ ,  $M$ , and  $Y$ , and, hence, the constraints are imposed on error filters in each of the three color planes. The error filter coefficients are a function of the input level  $d \in [0, 255]$ .

The design objective is to obtain error filter weights for each (C,M,Y) vector in the input. For 24-bit color images (with 8 bits per color plane), this would amount to a total of  $256^3$  input combinations. Designing this many error filters is impractical. Therefore, it is required to choose a limited number of CMY combinations that correspond to regions critical to color reproduction. We design error filters for CMY patches corresponding to the “true neutrals,” i.e., the locus  $(L^*, 0, 0)$  in CIELab space. There are two motivations for such an approach. First, the eye is particularly sensitive to colors near neutrals. Second, to a first-order approximation, the interaction among the colorants is taken into account.

### D. Color-Error Filter Design Procedure

Note that, while the Neugebauer printer model provides the characterization from device values to colorimetric values (e.g.,

	*	$h [0, 1; d]$
$h [1, -1; d]$	$h [1, 0; d]$	$h [1, 1; d]$

Fig. 6. FS support for the error filter, where \* denotes the current pixel.

CIELab), it is the inverse mapping from colorimetric (CIELab) values to device coordinates (CMY) that is sought for our purposes. Several researchers [48]–[51] have addressed the problem of inverting the Neugebauer equations. The inversion is a nonlinear problem that can be solved, in the case of three input colorants  $C$ ,  $M$ , and  $Y$  by iterative approaches. When the number of colorants exceeds three, the problem becomes ill posed, as several colorant combinations can result in the same measured color. However, from a practical viewpoint, that is not a concern since the amount of  $K$  or black in CMYK printers is determined by the gray-component replacement (GCR/UCR) strategy employed in the printer on top of known  $C$ ,  $M$ ,  $Y$  values. In this work, we used Chappuis’ approach [50] because it was designed specially for inversion of neutral colors.

The design procedure may then be summarized as follows.

- 1) Sample the 1-D locus  $(L^*, 0, 0)$  uniformly from  $(L_{\min}^*, 0, 0)$  to  $(L_{\max}^*, 0, 0)$ . where  $L_{\min}^*$  and  $L_{\max}^*$ , respectively, correspond to the minimum and maximum luminance

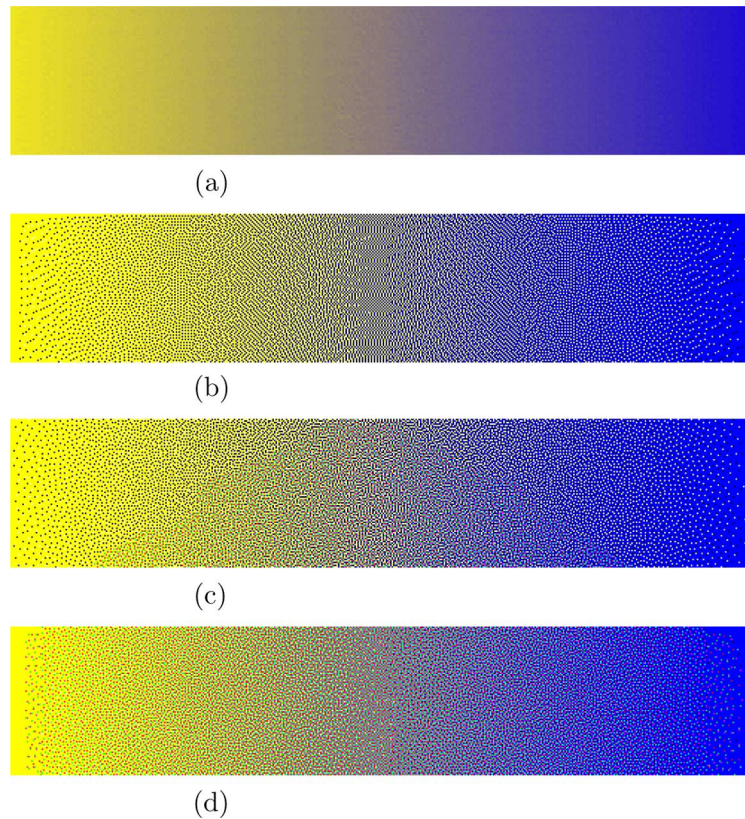


Fig. 7. Color ramp and its halftone images. The halftone in (c) is courtesy of Prof. J. P. Allebach and T.-C. Chang at Purdue University. (a) Original color ramp image. (b) FS error diffusion. (c) Separable application of grayscale TDED [24]. (d) Color TDED with serpentine scan.

values in the CIELab gamut of the printer. Let  $P$  denote the number of sampled triplets.

- 2) For each sampled triplet in Step 1), invert the printer model to obtain the  $C$ ,  $M$  and  $Y$  values needed to produce it. This will result in  $P$  combinations of CMY values.
- 3) Train the error filter weights to minimize the cost in (32) for each of these different CMY patches.
- 4) Interpolate between the filter coefficients corresponding to the  $P$  CMY patches to obtain error filters for  $C = 0, 1, 2 \dots 255$ ,  $M = 0, 1, 2 \dots 255$ , and  $Y = 0, 1, 2 \dots 255$ .

The aforementioned procedure results in 256 error filters for each color plane. We used  $P = 32$  and a spline interpolation between the filter coefficients. Empirically, we observed that using  $P > 25$  proved sufficient to generate an accurate estimate of the true/optimum filter coefficients for the intermediate  $C$ ,  $M$ , and  $Y$  digital levels. The individual  $C$ ,  $M$ , and  $Y$  values resulting from the inversion are plotted in Fig. 4 against uniformly sampled  $L^*$  values. It is quite clear from Fig. 4 that none of the three curves is close to linear. This is because equal CMY or  $C = M = Y$  rarely correspond to the (true) neutral axis in CIELab space. When this color TDED algorithm was first presented, we had proposed [52], [53] a design across the 1-D locus  $R = G = B$  for display applications.

Note that the TSE in (32), in general, is not a convex function. Hence, a global minimum cannot be guaranteed. The space of solutions (error filter weights), however, comprises a convex set. The algorithm to search for the error filter weights is sum-

marized in Fig. 5. It is an extension of Li and Allebach's search strategy [24] to multiple (i.e., three) dimensions. The design is based on a Floyd–Steinberg (FS) [8] support for the error filter (Fig. 6). This can, however, be easily generalized to error filters with other shapes and sizes.

## V. RESULTS AND ANALYSIS

### A. Evaluating Halftone Image Quality

Figs. 7 and 8 show color halftone images generated by 1) FS error diffusion, 2) grayscale TDED [24] applied separately to the  $C$ ,  $M$ , and  $Y$  color planes, and 3) the proposed color TDED method. The color TDED halftone in Fig. 7(d) does not suffer from directional artifacts such as diagonal worms. Worms can be seen in the FS halftone in the yellow and blue extremes of the ramp. False textures in the FS halftone are prominent in the middle of the yellow region (a third of the ramp length from the left) and in the center of the ramp (where yellow turns into blue). These are nearly absent in Fig. 7(d). The choice of color to render is also better for the color TDED halftone. In Fig. 7(b), white dots are rendered in the blue region. These are replaced by a mixture of magenta, cyan and black dots in the color TDED halftone which are less visible. By virtue of the Li and Allebach's design [24], traditional error-diffusion artifacts *viz.* worms and false textures are almost completely removed in Fig. 7(c).



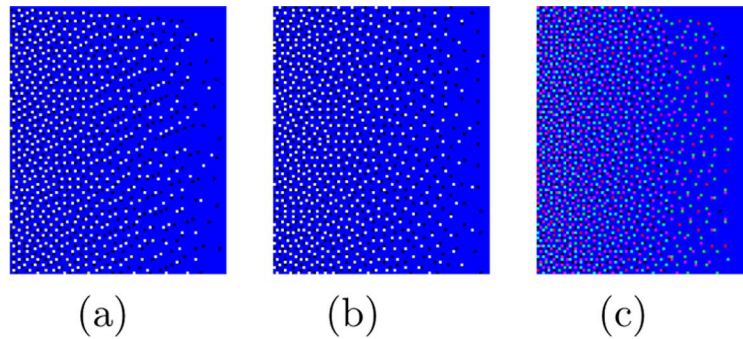


Fig. 8. Halftones of a portion of the blue section of the color ramp in Fig. 7(a). Grayscale TDED is applied separately to each color plane. (a) FS. (b) Grayscale TDED. (c) Color TDED.

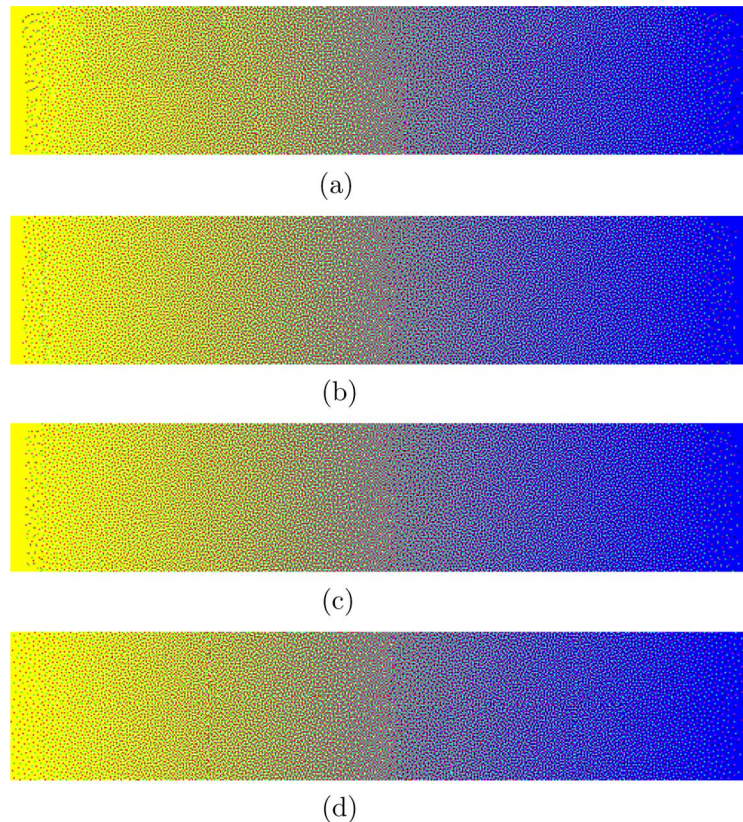


Fig. 9. Color ramp and its halftone images. The halftone in (d) is courtesy of Dr. J.-H. Lee at Hewlett-Packard and Prof. J. P. Allebach at Purdue University. (a) Color TDED with traditional raster scan. (b) Color TDED with 2-row serpentine scan. (c) Color TDED with serpentine scan. (d) Colorant-based direct binary search.

The halftone textures in Fig. 7(c) are also homogeneous.<sup>2</sup> However, the color rendition is similar to that of FS error diffusion in Fig. 7(b). This is expected because separable design for each color plane does not necessarily shape the color noise to frequencies of least visual sensitivity. Detail of the halftones in Fig. 7(b)–(d) are shown in Fig. 8(a)–(c). Note the significant improvement in the reduction of color halftone noise in Fig. 8(c) over Fig. 8(a) and (b).

Fig. 9 compares the halftones generated via color TDED using different scan paths and against the color direct binary

<sup>2</sup>All the images presented in this paper were converted to sRGB using a characterization from the CMY(K) of a HP laserjet printer for which the design was carried out. We request the readers to print these images to a color laserjet/inkjet printer with a resolution of 100 dots per inch or higher for a realistic visual estimate of the artifacts in print.

search (DBS) halftoning algorithm by Lee and Allebach [54]. The basic idea behind their halftoning method is to control the quality of each colorant texture separately along with the total dot distribution. In order to achieve this, the authors first set the total dot arrangement and then color the dots optimally without altering the total dot arrangement. Due to the computational complexity in the search for optimal dot arrangements and subsequent color selection (much like grayscale DBS), the algorithm in [54] cannot be directly used in real-time color printing paths but serves as a valuable upper bound on achievable color halftone quality. Hence, we treat the color halftone generated via this method Fig. 9(d) as a benchmark for our color TDED halftones. In fact, it can be seen that the color TDED and color DBS halftones in Fig. 9(a) and (d), respectively, are virtually indistinguishable. In particular, the choice of color to

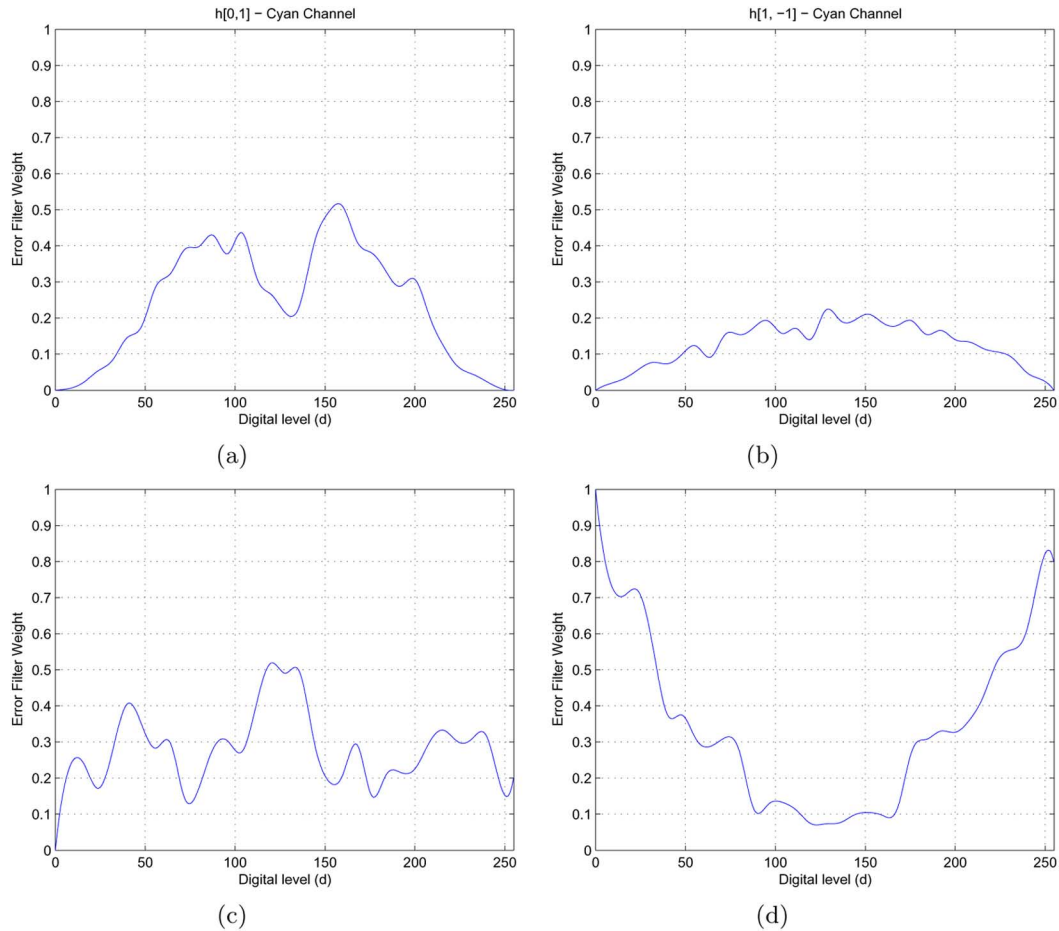


Fig. 10. Input-level-dependent error filter weights—Cyan channel. The values of these weights for the conventional FS filter are fixed at (a)  $h[0, 1] = (7/16)$ , (b)  $h[1, -1] = (3/16)$ , (c)  $h[1, 0] = (5/16)$ , and (d)  $h[1, 1] = (1/16)$ . (a)  $h[0, 1]$ , (b)  $h[1, -1]$ , (c)  $h[1, 0]$ , and (d)  $h[1, 1]$ .

render over the length of the ramp, is near identical for the two halftoning methods.

For color TDED, the conventional raster scan Fig. 9(a) still shows the tendency for dots to line up in horizontal or diagonal worms, particularly at extreme levels. Although the serpentine scan Fig. 9(c) almost completely removes directional artifacts, it can only be executed as a serial process. A two-row serpentine scan [24] employed in Fig. 9(b) generates comparable results to Fig. 9(c) but has more parallelism.

### B. Improved Noise Shaping via Input-Dependent Weights

Figs. 10–12 show for the  $C$ ,  $M$  and  $Y$  channels, respectively, the input-level or “tone” dependent optimized error filter coefficients based on a FS support for the error filter (Fig. 6). Two important observations may be made.

- 1) The error filter coefficients for each color plane are very different from the original FS coefficients in [8]. The deviation from FS coefficients is especially pronounced at extreme digital levels.
- 2) For each digital level, there is significant variation of the error filter coefficients across the three color planes.

Quantitatively, the second observation illustrates why applying even “optimized” grayscale error-diffusion halftoning

methods independently to each colorant plane will not result in accurate color rendition.

Fig. 13(b) and (c), respectively, shows halftone images of the *toucan* image in Fig. 13(a) generated by FS error diffusion and the proposed color TDED algorithm. As before, it may be seen that directional artifacts, e.g., diagonal worms that appear heavily in the FS halftone Fig. 13(b) are almost eliminated in Fig. 13(c). Further, the accuracy of color rendition is much higher in Fig. 13(c) as well, especially in the yellow color area on the body of the toucan on the left and close to the beak of the second toucan (on the right).<sup>3</sup>

Fig. 14 shows power spectral density (PSD) versus radial frequency plots for the FS and color TDED “error” images. These error images were computed by taking the difference of the original continuous tone image in Fig. 13(a) and the FS and color TDED halftone images in Fig. 13(b) and (c), respectively. In particular, Fig. 14(a) shows plots of PSD against radial frequency for the  $Y_y$  component of the FS and color TDED error images. Similar plots for the  $C_x$  and  $C_z$  components are shown in Fig. 14(b) and (c). The superior noise shaping

<sup>3</sup>When printed to a color printer, the colors may render slightly differently from what is described unless an accurate characterization from sRGB to the CMYK of the particular color printer is used. For comparison on an sRGB monitor, tiff versions can be obtained from: <http://www.ece.utexas.edu/~bevans/papers/2006/colorTDED/images.zip>

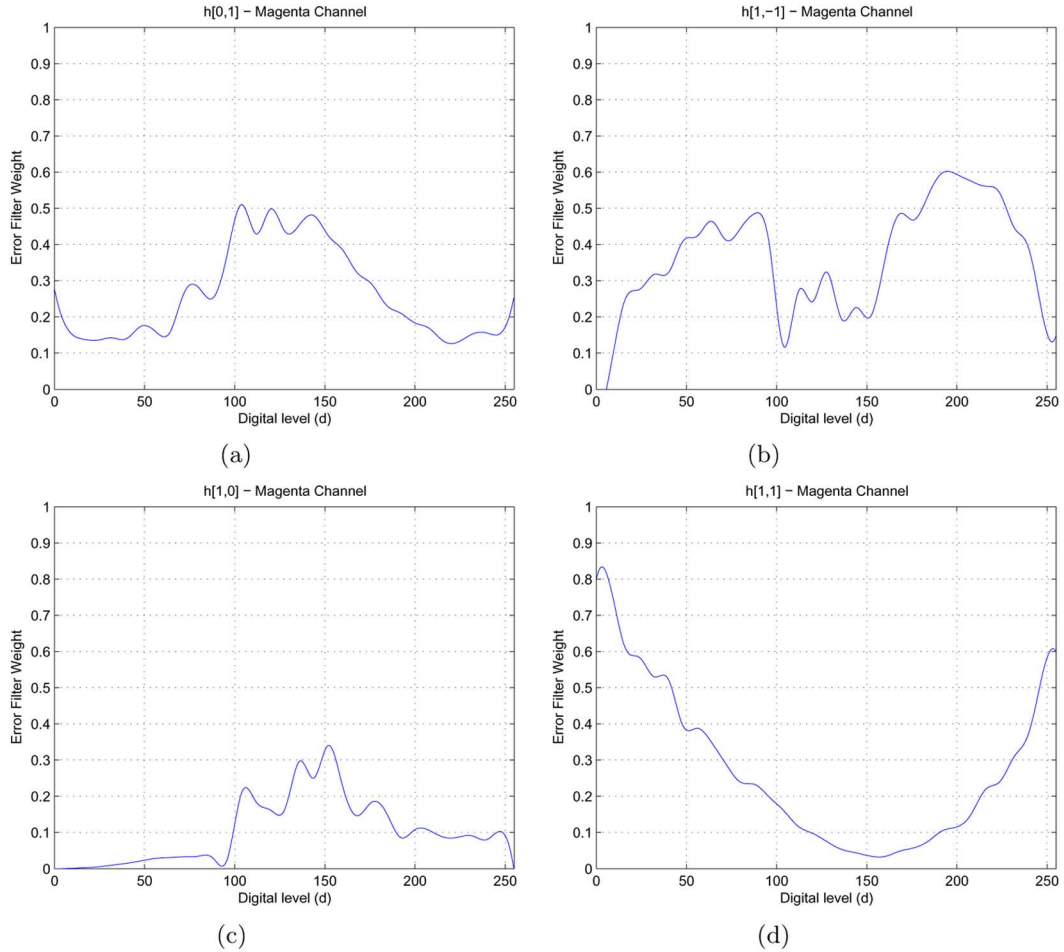


Fig. 11. Input-level-dependent error filter weights—Magenta channel. The values of these weights for the conventional FS filter are fixed at (a)  $h[0, 1] = (7/16)$ , (b)  $h[1, -1] = (3/16)$ , (c)  $h[1, 0] = (5/16)$ , and (d)  $h[1, 1] = (1/16)$ . (a)  $h[0, 1]$ , (b)  $h[1, -1]$ , (c)  $h[1, 0]$ , and (d)  $h[1, 1]$ .

behavior of color TDED is now readily apparent. Comparing the luminance PSD of FS and color TDED error images Fig. 14(a) it can be seen that the FS halftone has much more luminance error, which is readily perceived in the FS halftone image. Likewise, a comparison of the PSDs in Fig. 14(b) and (c) reveals that color TDED affords much higher chrominance error (especially at high radial frequencies). This illustrates that by using input-dependent color-error filters we are able to shape the color quantization noise primarily into high-frequency regions of the chrominance planes where the eye is least sensitive.

For any color image, we also provide an objective measure. The effective noise shaping gain (in decibels) of the color TDED halftones over the FS halftones may be computed as

$$NG = 10 \log_{10} \left( \frac{TSE_{FS}}{TSE_{colorTDED}} \right) \quad (34)$$

where  $TSE_{FS}$  denotes the total squared error in (32) computed for a FS halftone image against the original.  $TSE_{colorTDED}$  is similar. Table I tabulates the noise gain of color TDED over FS halftones for four standard test images.

## VI. ENHANCEMENTS

In addition to using error filter weights that depend on the input level, error filter shape and size may also be varied for dif-

fusion of errors. Li and Allebach [24] use wider matrices to improve rendering of shadow and highlight regions. With a wider matrix, the current pixel to be binarized will be affected by a larger area of the halftone region.

Fig. 15 shows color-error filter shapes (for each color plane) that are dependent on the input level  $d \in [0, 255]$ . In our design, the maximum number of filter coefficients was limited to four (as in FS [8] error diffusion) but the locations of the filter weights were chosen (empirically) based on the input digital level. The results presented in Fig. 13 use the error filter shapes in Fig. 15.

Many other approaches reduce directional artifacts in error diffusion. Fan proposed an error weighting matrix that allows the quantizer error to propagate farther back on the next line to reduce worm artifacts [55]. As discussed in Section I, other approaches used larger error-weighting matrices/filters for highlight and shadow regions [21], [56]. These ideas may all be combined into optimizing color-error filters dependent on the input CMY triplets using the proposed design framework.

## VII. CONCLUSION

We propose a model-based color-error diffusion halftoning algorithm with error filter weights optimized dependent

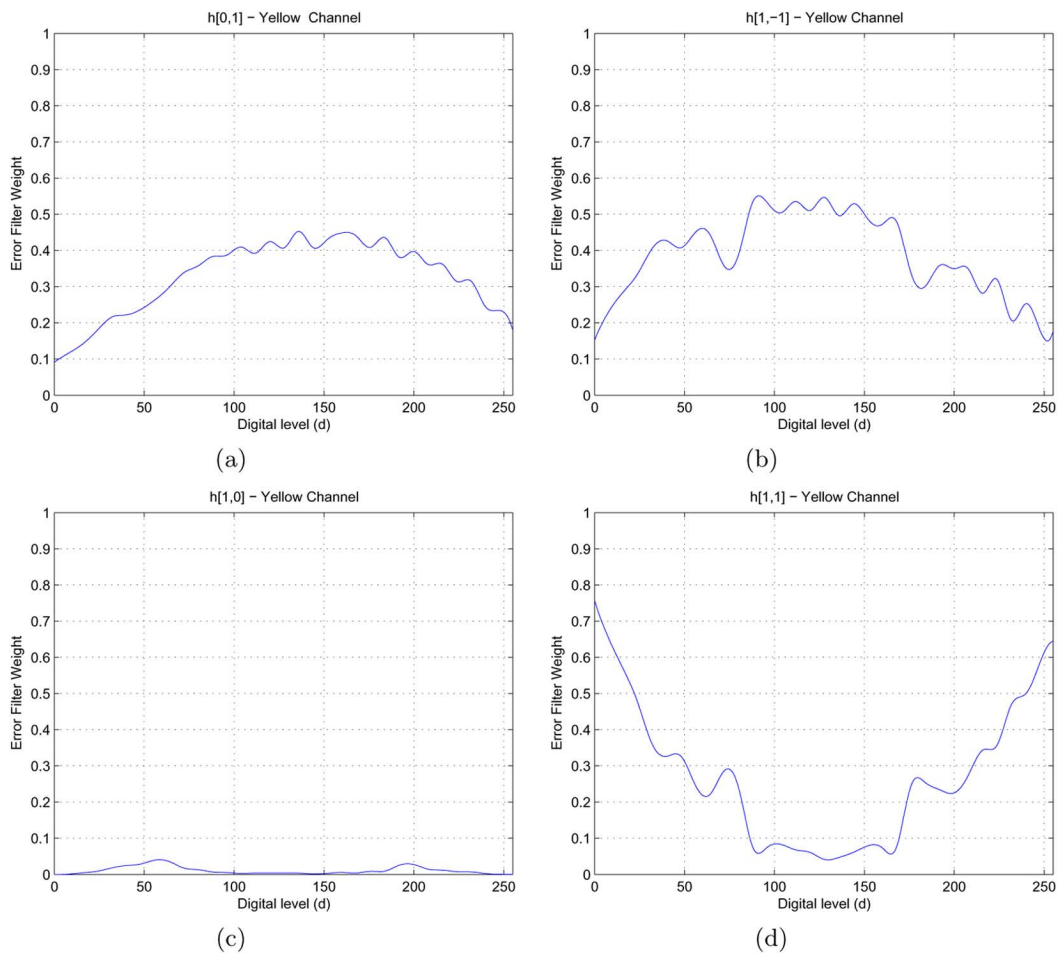


Fig. 12. Input-level-dependent error filter weights—Yellow channel. The values of these weights for the conventional FS filter are fixed at (a)  $h[0, 1] = (7/16)$ , (b)  $h[1, -1] = (3/16)$ , (c)  $h[1, 0] = (5/16)$ , and (d)  $h[1, 1] = (1/16)$ . (a)  $h[0, 1]$ , (b)  $h[1, -1]$ , (c)  $h[1, 0]$ , and (d)  $h[1, 1]$ .

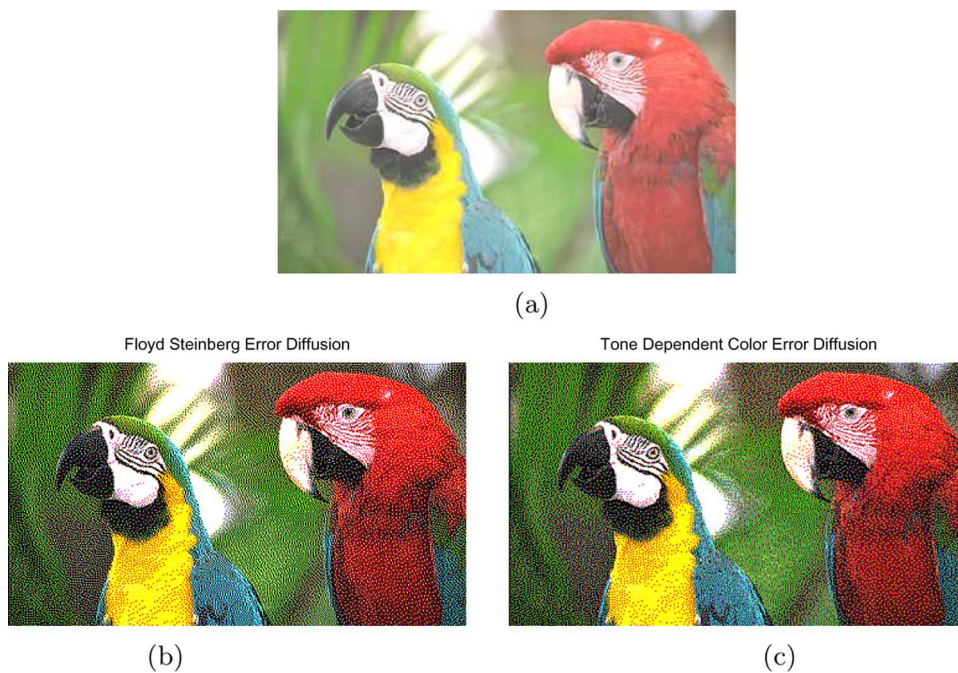


Fig. 13. FS and color TDED halftones of the toucan image. (a) Original 24-bit toucan image. (b) FS error diffusion. (c) Color TDED.

on the input CMY triplet. Our design procedure trains color-error filters for CMY combinations corresponding to the “true”

neutrals in CIELab space. The resulting halftones exhibit significantly enhanced color noise shaping and achieve halftone

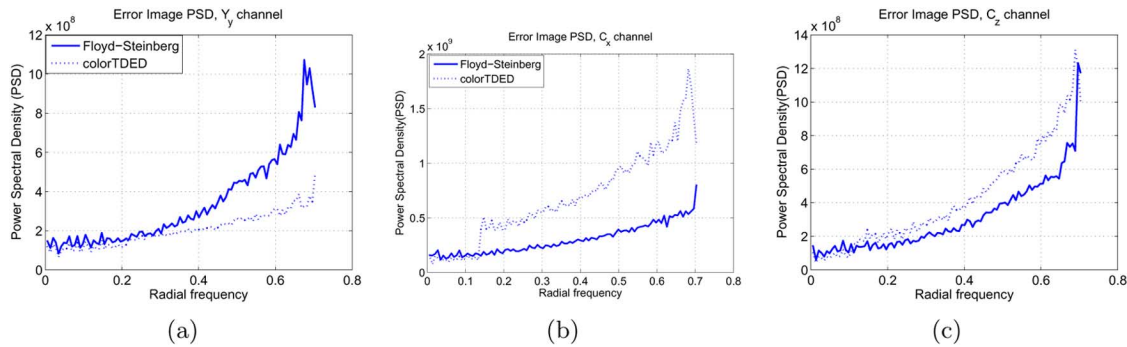


Fig. 14. Power spectral density of the FS and color TDED error images:  $Y_y$ ,  $C_x$ , and  $C_z$  components. (a) Error image:  $Y_y$  component. (b) Error image:  $C_x$  component. (c) Error image:  $C_z$  component.

TABLE I  
NOISE GAIN (IN DECIBELS) OF THE COLOR TDED WEIGHTS OVER  
THE FS FILTER ON FOUR STANDARD TEST IMAGES

Image	Noise gain (dB)
lena	4.1172
peppers	3.2489
house	5.0077
pasta	4.5550

## REFERENCES

- [1] R. Ulichney, "Dithering with blue noise," *Proc. IEEE*, vol. 76, no. 1, pp. 56–79, Jan. 1988.
- [2] T. Mitsa and K. Parker, "Digital halftoning using a blue noise mask," *J. Opt. Soc. Amer. A*, vol. 9, no. 11, pp. 1920–1929, Nov. 1992.
- [3] R. Ulichney, "The void-and-cluster method for dither array generation," in *Proc. SPIE Human Vision, Visual Processing, and Digital Display IV*, Feb. 1993, vol. 1913, pp. 332–343.
- [4] C. Hains, S. Wang, and K. Knox, *Digital Color Halftones, Chapter 6 in Digital Color Imaging Handbook*, G. Sharma, Ed. Boca Raton, FL: CRC, 2003.
- [5] M. Analoui and J. P. Allebach, "Model based halftoning using direct binary search," presented at the SPIE Human Vision, Visual Processing, and Digital Display III, Feb. 1992.
- [6] S. H. Kim and J. P. Allebach, "Impact of human visual system models on model based halftoning," *IEEE Trans. Image Process.*, vol. 11, no. 3, pp. 258–269, Mar. 2002.
- [7] J. P. Allebach and Q. Lin, "FM screen design using the DBS algorithm," in *Proc. IEEE Conf. Image Processing*, Sep. 1996, vol. I, pp. 539–542.
- [8] R. Floyd and L. Steinberg, "An adaptive algorithm for spatial grayscale," *Proc. Soc. Image Display*, vol. 17, 1976.
- [9] R. Ulichney, *Digital Halftoning*. Cambridge, MA: MIT Press, 1987.
- [10] B. L. Evans, V. Monga, and N. Damera-Venkata, "Variations on error diffusion: Retrospectives and future trends," in *Proc. SPIE Color Imaging: Processing, Hardcopy and Applications VIII*, Jan. 2003, vol. 5008, pp. 371–389.
- [11] C. Billotet-Hoffman and O. Brynghdahl, "On the error diffusion technique for electronic halftoning," *Proc. Soc. Inf. Display*, vol. 24, pp. 253–258, 1983.
- [12] R. L. Miller and C. M. Smith, "Image Processor With Error Diffusion Modulated Threshold Matrix," U.S. Patent 5 150 429, Sep. 1992.
- [13] R. Levien, "Output dependent feedback in error diffusion halftoning," *IS&T Imag. Sci. Technol.*, vol. 1, pp. 115–118, May 1993.
- [14] J. Sullivan, R. Miller, and G. Pios, "Image halftoning using a visual model in error diffusion," *J. Opt. Soc. Amer. A*, vol. 10, no. 8, pp. 1714–1724, Aug. 1993.
- [15] R. Eschbach, "Error-diffusion algorithm with homogeneous response in highlight and shadow areas," *J. Electron. Imag.*, vol. 6, pp. 1844–1850, Jul. 1997.
- [16] N. Damera-Venkata and B. L. Evans, "Adaptive threshold modulation for error diffusion halftoning," *IEEE Trans. Image Process.*, vol. 10, no. 1, pp. 104–116, Jan. 2001.
- [17] P. Wong, "Adaptive error diffusion and its application in multiresolution rendering," *IEEE Trans. Image Process.*, vol. 5, no. 7, pp. 1184–1196, Jul. 1996.
- [18] B. Kolpatzik and C. Bouman, "Optimized error diffusion for high quality image display," *J. Electron. Imag.*, vol. 1, pp. 277–292, Jan. 1992.
- [19] P. W. Wong and J. P. Allebach, "Optimum error diffusion kernel design," presented at the SPIE/IS&T Symp. Electron. Imag., Jan. 1997.
- [20] I. Witten and R. Neal, "Using peano curves for bilevel display of continuous-tone images," *IEEE Comput. Graph. Appl.*, vol. 2, no. 3, pp. 47–51, May 1982.
- [21] R. Eschbach, "Reduction of artifacts in error diffusion by means of input-dependent weights," *J. Electron. Imag.*, vol. 2, no. 4, pp. 352–358, Oct. 1993.
- [22] J. Shu, "Adaptive filtering for error diffusion by means of input-dependent weights," in *Proc. SID Dig. Tech. Papers*, May 1995, pp. 833–836.

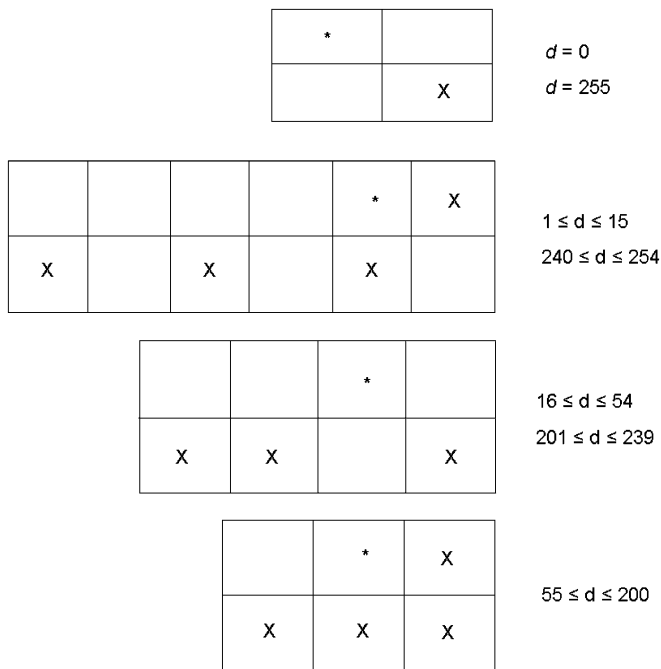


Fig. 15. Input level-dependent error filters for color TDED with serpentine scan, where \* denotes the current pixel.

quality approaching that of CMY(K) color DBS [54]. An interesting direction for future work is to explore the best possible canonical CMY patches along which to design the color-error filters.

- [23] V. Ostromoukhov, "Enhanced Error-Diffusion Method for Color or Black-and-White Reproduction," U.S. Patent 737 453, 1998.
- [24] P. Li and J. P. Allebach, "Tone dependent error diffusion," in *Proc. SPIE Color Imaging: Device Independent Color, Color Hardcopy, and Applications VII*, Jan. 2002, vol. 4663, pp. 310–321.
- [25] N. Damera-Venkata, B. L. Evans, and V. Monga, "Color error diffusion," *IEEE Signal Process. Mag.*, vol. 20, no. 4, pp. 51–58, Jul. 2003.
- [26] R. V. Klassen and R. Eschbach, "Vector error diffusion in a distorted color space," presented at the IS & T Conf. 47th Annu. Conf, May 1994.
- [27] H. Haneishi, T. Suzuki, N. Shimonyama, and Y. Miyake, "Color digital halftoning taking colorimetric color reproduction into account," *J. Electron. Imag.*, vol. 5, no. 1, pp. 97–106, Jan. 1996.
- [28] Z. Fan and S. Harrington, "Improved quantization methods in color error diffusion," *J. Electron. Imag.*, vol. 8, no. 4, pp. 430–437, Oct. 1999.
- [29] C. Kim, I. Kweon, and Y. Seo, "Color and printer models for color halftoning," *J. Electron. Imag.*, pp. 166–180, Jun. 1997.
- [30] N. Damera-Venkata and B. L. Evans, "Design and analysis of vector color error diffusion halftoning systems," *IEEE Trans. Image Process.*, vol. 10, no. 10, pp. 1552–1565, Oct. 2001.
- [31] V. Monga, W. S. Geisler, and B. L. Evans, "Linear, color separable, human visual system models for vector error diffusion halftoning," *IEEE Signal Process. Lett.*, vol. 10, no. 4, pp. 93–97, Apr. 2003.
- [32] G. Sharma, *Digital Color Imaging Handbook*. Boca Raton, FL: CRC, 2002.
- [33] T. J. Flohr, B. W. Kolpatzik, R. Balasubramanian, D. A. Carrara, C. A. Bouman, and J. P. Allebach, "Model based color image quantization," presented at the SPIE Human Vision, Visual Processing and Digital Display IV, 1993.
- [34] J. Mannos and D. Sakrison, "The effects of a visual fidelity criterion on the encoding of images," *IEEE Trans. Inf. Theory*, vol. 20, no. 4, pp. 525–536, Jul. 1974.
- [35] V. Ostromoukhov, "A simple and efficient error-diffusion algorithm," presented at the Int. Conf. Computer Graphics and Interactive Technology, Aug. 2001.
- [36] D. Shaked, N. Arad, A. Fitzhugh, and I. Sobel, "Ink relocation for color halftones," HPL-96-127R1, HP Labs Tech. Rep., 1996.
- [37] ———, "Color Diffusion: Error-Diffusion for Color Halftones," HPL-96-128R1, HP Labs Tech. Rep., 1996.
- [38] T. D. Kite, B. L. Evans, and A. C. Bovik, "Modeling and quality assessment of halftoning by error diffusion," *IEEE Trans. Image Process.*, vol. 9, no. 4, pp. 909–922, May 2000.
- [39] W. Rhodes, "Fifty years of the neugebauer equations," *Proc. SPIE*, pp. 7–18, 1989.
- [40] R. Balasubramanian, "Optimization of the spectral neugebauer model for printer characterization," *J. Electron. Imag.*, vol. 8, pp. 156–166, Apr. 1999.
- [41] J. A. C. Yule, *Principles of Color Reproduction*. New York: Wiley, 1967.
- [42] J. A. C. Yule and W. J. Nielsen, "The penetration of light into paper and its effect on halftone reproduction," in *Proc. Technical Association of the Graphic Arts Annu. Conf.*, Sep. 1951, pp. 65–71.
- [43] M. Pearson, " $N$  value for general conditions," in *Proc. Technical Association of the Graphic Arts Annu. Conf.*, Sep. 1980, pp. 415–425.
- [44] K. T. Mullen, "The contrast sensitivity of human color vision to red-green and blue-yellow chromatic gratings," *J. Physiol.*, vol. 359, pp. 381–400, 1985.
- [45] "What is sRGB?—Introduction to the Standard Default RGB Color Space Developed by Hewlett-Packard and Microsoft," 1999 [Online]. Available: <http://www.srgb.com/aboutsrgb.html>
- [46] J. Sullivan, L. Ray, and R. Miller, "Design of minimum visual modulation halftone patterns," *IEEE Trans. Syst., Man, Cybern.*, vol. 21, no. 1, pp. 33–38, Jan. 1991.
- [47] D. H. Kelly, "Spatiotemporal variation of chromatic and achromatic contrast thresholds," *J. Opt. Soc. Amer. A*, vol. 73, pp. 742–750, Jun. 1983.
- [48] I. Pobboravsky, "Methods of computing ink amounts to produce a scale of neutrals for photomechanical reproduction," in *Proc. Technical Association of the Graphic Arts Annu. Conf.*, Sep. 1966, pp. 10–34.
- [49] I. Pobboravsky and M. Pearson, "Computation of dot areas required to match a colorimetrically specified color using the modified neugebauer equations," in *Proc. Technical Association of the Graphic Arts Annu. Conf.*, Sep. 1972, pp. 65–77.
- [50] P. H. Chappuis, "A modified factorization of the neugebauer equations to compute accurate mask characteristics for neutral balance," in *Proc. Technical Association of the Graphic Arts Annu. Conf.*, Sep. 1977, pp. 256–280.
- [51] M. Mahy and P. Delbasita, "Inversion of the neugebauer equations," *Color Res. Appl.*, pp. 404–411, Jun. 1996.

- [52] V. Monga, N. Damera-Venkata, and B. L. Evans, "An input-level dependent approach to color error diffusion," in *Proc. SPIE Color Imaging: Processing, Hardcopy and Applications IX*, Jan. 2004, vol. 5009, pp. 333–343.
- [53] V. Monga and B. L. Evans, "Tone dependent color error diffusion," in *Proc. IEEE Int. Conf. Acoustics, Speech, and Signal Processing*, May 2004, vol. 3, pp. 101–104.
- [54] J.-H. Lee and J. P. Allebach, "Colorant based direct binary search halftoning," *J. Electron. Imag.*, vol. 11, pp. 517–527, Oct. 2002.
- [55] Z. Fan, "A simple modification of error diffusion weights," in *Proc. IS&T 46th Annu. Conf.*, May 1993, pp. 113–114.
- [56] P. Stucki, "MECCA—A Multiple-Error Correcting Computation Algorithm for Bilevel Hardcopy Reproduction," Res. Rep. RZ1060, IBM Res. Lab., Zurich, Switzerland, 1981.



**Vishal Monga** (S'97–M'06) received the B.Tech. degree in electrical engineering from the Indian Institute of Technology (IIT), Guwahati, in May 2001, and the M.S.E.E. and Ph.D. degrees from The University of Texas, Austin, in May 2003 and August 2005, respectively.

He is currently a Member of Research Staff in the Xerox Wilson Research Center, Webster, NY. His research interests span statistical signal and image processing, applied linear algebra, and probability. He has researched problems in color imaging, particu-

larly halftoning and device color correction, perceptual media hashing, and multimedia security.

Dr. Monga is a member of SPIE and IS&T. He received the IS&T Raymond Davis scholarship in 2004, a Texas Telecommunications Consortium (TxTec) Graduate Fellowship from The University of Texas for the year 2002 to 2003, and the President's Silver Medal in 2001 from IIT, Guwahati.



**Niranjan Damera-Venkata** (S'96–M'06) received the B.E. degree in electronics and communication engineering from the University of Madras, India, in 1997, and the M.S. and Ph.D. degrees in electrical engineering from the University of Texas at Austin in 1999 and 2000, respectively.

Since July 2000, he has been with Hewlett-Packard Laboratories, Palo Alto, CA, where he is currently a Senior Scientist in the Media Technology Lab. He contributed key theory and image processing algorithms to HP's "wobulation" technology that enables

high-quality resolution doubling of projection displays. He has also published works in areas such as digital halftoning, document security, symbolic design, image/video quality assessment, and camera image processing. His current research interests lie in applying computer graphics, computer vision, signal processing, and color science to a wide range of display-rendering problems.

Dr. Damera-Venkata is a member of Sigma Xi.



**Brian L. Evans** (SM'97) received the B.S.E.E.C.S. degree from the Rose-Hulman Institute of Technology, Terre Haute, IN, in 1987, and the M.S.E.E. and Ph.D.E.E. degrees from the Georgia Institute of Technology, Atlanta, in 1988 and 1993, respectively.

From 1993 to 1996, he was a Postdoctoral Researcher at the University of California, Berkeley. Since 1996, he has been with the Department of Electrical and Computer Engineering at The University of Texas, Austin, where he is currently a Professor. In signal processing, his research group

is focused on the design and real-time software implementation of wireless OFDM base stations and ADSL transceivers for high-speed Internet access. His group developed the first time-domain equalizer training method that maximizes a measure of bit rate and is realizable in real time in fixed-point software. In image processing, his group is focused on the design and real-time software implementation of high-quality halftoning for desktop printers, multimedia security and search, and smart image acquisition for digital still cameras.

Dr. Evans is a member of the Design and Implementation of Signal Processing Systems Technical Committee of the IEEE Signal Processing Society. He is the recipient of a 1997 U.S. National Science Foundation CAREER Award.